Beam propagation in Cu^+-Na^+ ion exchange channel waveguides

L.J. Villegas-Vicencio, A.V. Khomenko, D. Salazar, and H. Márquez
Departamento de Óptica, Centro de Investigación Científica y de Eduación Superior de Ensenada Km. 107 carretera Tijuana-Ensenada, Ensenada, Baja California, Mexico

H. Porte
Laboratorie d'Optique, P.M. Duffieux, UMR 6603, CNRS, Université de Franche-Comté, UFR des Sciences et Techniques 16 Route de Gray, 25030, Besançon, Cedex, France

Recibido el 25 de septiembre de 2000; aceptado el 2 de febrero de 2001

We employ the fast Fourier transform beam propagation method to simulate the propagation of light in graded index channel waveguides, these have been obtained by solid state diffusion of copper ions in soda-lime glass substrates. Longitudinal propagation has been simulated, the input light beam has a gaussian profile. Two cases have been analyzed, in the first, the Gaussian beam is colinear center to center with respect to waveguide; in the second, a small lateral offset and angular tilt have been introduced. Modal beating and bending effects have been founded. We have proven the validity of our numerical results in detailed comparison with experimental data.

Keywords: Graded index optics; channel waveguides; FFT-BPM; beam propagation method

Se ha empleado el método de propagación de haces por la transformada rápida de Fourier para simular la propagación de la luz en guías de onda de índice de gradiente. Éstas han sido fabricadas por difusión de iones de cobre en estado sólido en substratos de vidrios sódico-cálcicos. Se han simulado dos casos; el primero, el perfil de luz de entrada, que es gaussiano, es colineal centro a centro respecto al centro de la guía de ondas; el segundo, se ha dado un pequeño corrimiento lateral y una inclinación angular. Como consecuencia de los casos anteriores se ha observado efectos de batimiento modal. Los resultados de la simulación se han validado con resultados experimentales.

Descriptores: Índice de gradiente; guías de onda angostas; FFT-BPM; método de propagación de haces

PACS: 42.82.E; 42.79.Ry; 43.82.Et; 42.82.Cr; 07.05.Tp

1. Introduction

Ion exchanged glass waveguides play an important role in development of passive integrated optical components for fiber-optic communications and optical sensors [1, 2]. It is of great importance to have powerful and flexible tools of analysis to design, simulate and optimize dielectric structures. Numerical techniques must generally be employed to investigate light propagation in such devices. The most popular approach is a spectral procedure known as the beam propagation method (BPM) [3].

Optical waveguide problems are typically divided into two distinct classes. For waveguides, whose cross sectional dimensions and index profiles do not vary along the direction of propagation, called z-invariant waveguides, optical propagation can be described in terms of normal optical modes. The simplest method for these waveguides is the so-called effective index method [4]. For waveguides geometries varying along the propagation direction, called z-variant waveguides structures, general modeling tools are BPMs [5].

The BPM is now widely accepted as one of the most powerful methods for analyzing waveguides, because the calculation of optical fields using the BPM is almost always successful and for certain problems it is the only way to obtain the results [6, 7]. The BPM is a stepwise algorithm, consisting essentially of replacing the optical propagation in an inhomogeneous and/or nonlinear medium by a beam propagation through a sequence of homogeneous thin layers with phase/polarization correction after each layer. These corrections introduce the entire information about optical nonuniformity and nonlinearity of a layer by a single phase and polarization correction. The first BPM includes essentially the fast Fourier transform to convert the optical field from the coordinate to space frequencies domain and back. Nowadays this version is known as FFT-BPM. Afterwards, another BPMs, such as finite difference (FD-BPM) and finite elements (FE-BPM) were developed [8, 9]. In the past BPM has limited to solving the scalar wave equation, but it was extended recently to solve the vector wave equation that allows the analysis of the polarization evolution in linear and nonlinear medium [10–12].

A lot of works on modeling rib waveguides have been realized, which are based on FE-BPM [13–15] and FD-BPM algorithms [3, 4, 9, 13, 16–24], and yet are continuously innovated. However, much less work has been done on gradient index waveguides and, in particular, it has not been made a comparison between experimental and modeling results. In this paper, we present the results on a numerical simulation of the light propagation in a single-mode and multi-mode channel graded index waveguides. We compare this results with the results of our experiments. The paper is organized in three main parts (following the introduction): in Sec. 2, the employed numerical method is discussed. In Sec. 3 the ion diffusion process involved in waveguide fabrication is described. Section 4 includes a comparison between our numerical and experimental results. Finally, we present the conclusions for our work in Sec. 5.

2. Numerical method

In this paper we take forward light propagation through a graded index channel waveguide, they were fabricated in glass substrates by thermal diffusion assisted by electric field [25]. These are weakly guided waveguides and can be properly described by two-dimensional BPM algorithm [7, 26]. Moreover, recent studies on rib waveguides show that, for practical purpose, the scalar solutions with polarization corrections are just as accurate as the vectorial solutions obtained from the finite element and finite difference methods. That is why the scalar analysis, with polarization correction if necessary, turns out to be the most economical approach to meet most of needs in modeling passive integrated optics [6].

The calculation starts with the definition of the input wave distribution, $E(x,0)$, in a plane at the device input facet, given as field values in discrete grid points. The coordinate system is defined such that z is the light propagation direction, *i.e.* the longitudinal direction, and x is the transverse direction. Then the kernel of FFT-BPM is executed including the following steps:

a) The angular spectra is multiplied by propagator P, that corresponds to the wave propagation on half of the interval, $\Delta z/2$.

b) The angular spectra is transformed back into position space.

c) The phase is corrected by multiplied on a coordinate space operator Φ.

d) The optical field is transformed into angular spectra.

e) The angular spectra is propagated by second half step, $\Delta z/2$, the calculation is repeated stepwise.

An expression that relates the optical fields at two planes separated by the distance Δz, can be written in an operatorial form as

$$E(x, z+\Delta z) = F^{-1}PF\Phi F^{-1}PFE(x,z), \qquad (1)$$

where $E(x,z)$ represents the electric field in cartesian spatial coordinates; F and F^{-1} are, respectively, the operators of direct and inverse fast Fourier transform. Operator P allows to calculate the effect of the light propagation through the uniform media with a constant refractive index n_0. This operator becomes a simple phase factor in the domain of the spatial frequencies. The operator Φ is to introduce a phase correction taking into account the variation of the refractive index. It takes a form of phase factor in the coordinate domain [7, 27]. Both operators are defined as follows:

$$P = \exp\left[-i\frac{\Delta z}{2}\left(\frac{k_\perp^2}{k+\sqrt{k_\perp^2+k^2}}\right)\right], \qquad (2)$$

$$\Phi = \exp\left[-i\Delta z\frac{k\delta n}{n_0}\right], \qquad (3)$$

where δn denotes the variation of the refractive index, n_o is the reference refractive index, $k = 2\pi n_0/\lambda$ is the wavenumber and $k_\perp$ is the length of the transverse component of the wavevector.

Because inherent nature of FFT algorithm, in order to avoid that the optical field that reaches the edge of the computational window in transverse direction be folded back to the opposite edge of the window, causing high-frequency numerical instabilities, we have used the method of a smooth absorber function at each propagation step [28].

3. Waveguide fabrication

The waveguides were fabricated by an electric-field assisted Cu^+-Na^+ ion exchange in soda-lime glass substrate. Corning 2947 glass substrates was selected because they have an elevated percentage of sodium ($\sim$15% wt.), which facilitate Cu^+-Na^+ ion exchange. In this process, both cations that exchange each other are network modifiers. The ionic radius for Cu^+ is 0.96 Å which is similar to the Na^+ of 0.95 Å [29]. As a result, the basic glass structure almost does not suffer a perturbation due to ion exchange, while the glass refractive index is modified. The change in refractive index is taken to be proportional to the Cu^+ concentration induced into the glass, which in turn is proportional to the initial condition of Na^+.

Such as mentioned above, the refraction index maximum increment should be much small to substrate refractive index, that is the weakly guiding condition, which is important for an implementation of BPM. Mathematically is described as follows:

$$\left|\frac{n_0^2 - n_s^2}{n_0^2}\right| \ll 1. \qquad (4)$$

Glass substrates used in our experiment have a refractive index of $n_0 = 1.514$, and the maximum increment in the waveguide is $\Delta n = 0.052$ [30], then the maximum waveguide refractive index reaches a value of $n_s = 1.566$, substituting these values in Eq. (4) a value of 6.98×10^{-2} is obtained, which it is clearly much smaller than 1, and therefore the weakly guided condition is fulfilled [31].

A standard photolithographic technique was used to make the mask openings in a titanium layer on the glass substrate. The mask contains 4 cm long and 4 μm wide lines, with separation between adjacent lines of 100 μm. Details about diffusion technique can be found in Ref. 30.

A copper film with thickness of approximately 1 μm was deposited on the 1 mm thick glass substrate as Cu^+ ion source. To assist the diffusion an electric field of 30 V/mm was applied to the substrate during 1 hr at 623 K. After the diffusion procedure, the end faces of the substrate were polished. Figure 1 shows a typical microphotograph of the end face with the waveguide. The substrate was illuminated by the tungsten lamp through the opposite end face of the substrate.

Simulation results of the copper ions diffusion process in a glass substrate is shown in Fig. 2. This simulation [32] is

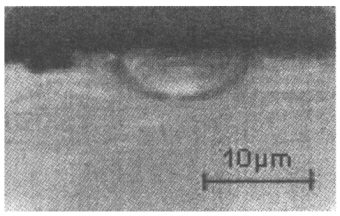

FIGURE 1. Microphotograh of the waveguide. Its dimensions are about 10 μm width and 4 μm depth.

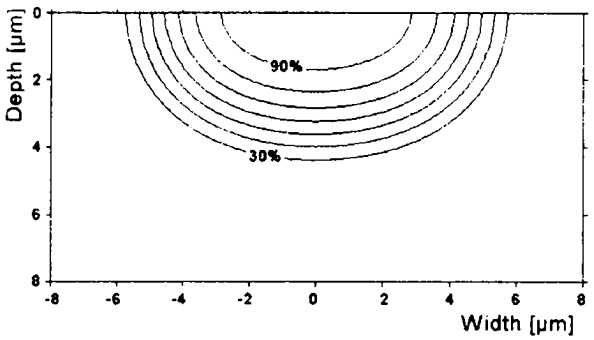

FIGURE 2. Distrbution of the copper in the substrate. Contours corresponds to the constant ion concentration with 100% increment.

based in following equation:

$$\frac{\partial C}{\partial t} = \frac{D\nabla^2 C}{C(M-1)+1} - \frac{D(M-1)(\nabla C)^2 + M\,\overline{J_0}\,\nabla C}{[C(M-1)+1]^2}, \quad (5)$$

which represents a change of concentration with time in the electric field assisted diffusion process. Here M is the ratio of the self diffusion constant from the exchange ions, D is the diffusion coefficient of incoming ions, C is the relative concentration, and $\overline{J_0}$ is the electric current density. Our principal simulation values are $D = 5.39 \times 10^{-16}$ m^2/s; $M = 0.19$; $C = 0.89$; $\overline{J_0} = 100$ μA/cm^2; 4 μm ion source strip width by 1 μm thickness. Diffused channel waveguide and calculated contours concentration profiles are shown in Figs. 1 and 2 respectively, have good agreement in dimensions, both are about 10 μm wide by 4 μm depth.

Figure 2 shows the copper concentration as a function of the waveguide width and depth. The variation of the refractive index is proportional to the copper concentration, thus the index variation are similar to the presented in Fig. 3. One can see that waveguide depth is smaller than its width of approximately 2.5 times. Figure 4 shows the distribution of the refractive index in the width direction.

4. Numerical and experimental results

In this section we present the results of an analysis of light propagation in straight graded index channel waveguides. We discuss three different cases. The first one is related with propagation of light in the glass substrate with two parallel channel waveguides when the whole input face of the substrate is

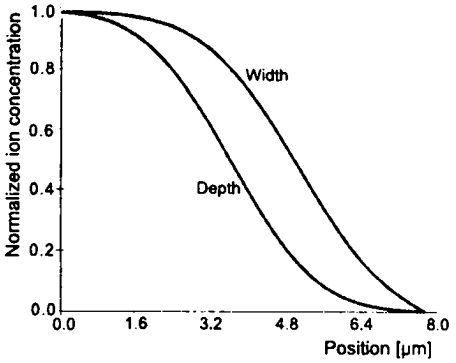

FIGURE 3. Normalized ion concentration profiles in width and depth directions.

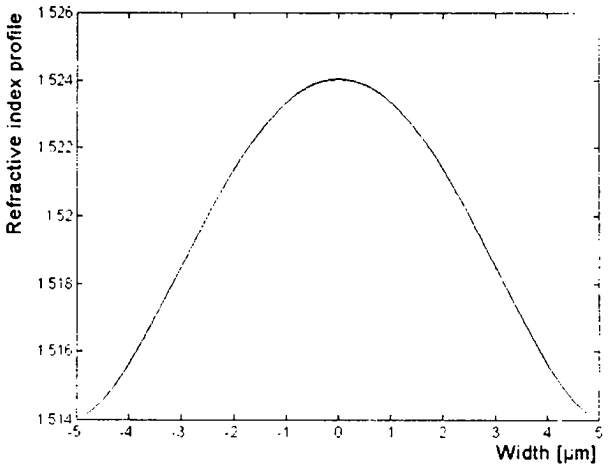

FIGURE 4. Refractive index variation in the width direction close to the substrate surface.

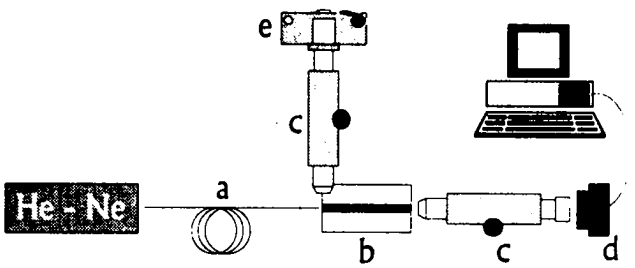

FIGURE 5. Experimental setup: a) optical fiber, b) channel waveguide, c) microscopes, d) CCD camera, and e) photographic camera.

illuminated by a plane wave. The second and third are dedicated to analyze the light coupling and discuss the peculiarities of the light propagation in the waveguide associated with a mutual lateral shift and angular tilt between the coupled beam and channel waveguide. All three cases was numerically realized by FFT-BPM and compared with experimental results.

Our experimental setup is shown in Fig. 5. Light of a He-Ne laser (632.8 nm) was coupled to our waveguides through a monomodal optical fiber. Sample and optical fiber

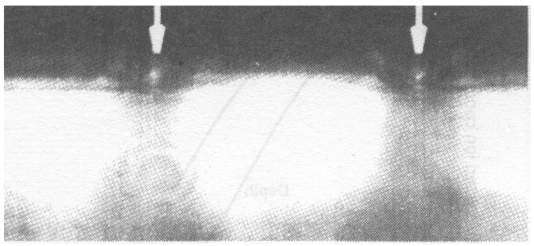

FIGURE 6. White arrows indicate the emergent guided light in two graded index channel waveguide separated 100 μm center to center.

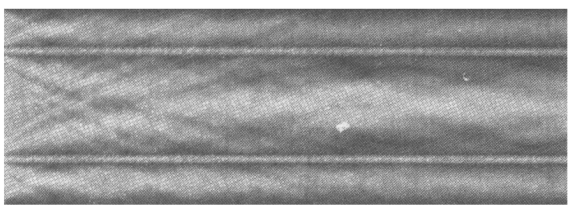

FIGURE 7. Image result of the simulation of light propagation in a substrate containing two graded index channel waveguides. The light is a plane monochromatic wavefront. Light propagates from left to right.

were aligned using a micromechanical mount to obtain efficient coupling. A microscope located above the sample was guide. The same microscope allowed us to take the photographs of the top surface of the substrate. Another microscope was used to record the images of the substrate using a CCD camera.

Figure 6 shows a photograph of the end face of the substrate, that was taken when the whole opposite end face was illuminated by a He-Ne laser beam. The white arrows show the locations of the waveguide outputs, where one can see a bright spot formed by the guided light. Each waveguide is surrounded by a dark area, which allows easily locating the waveguide output.

Figure 7 presents the calculation of two-dimensional distribution of the light intensity in the xz plane. It shows how propagating light should be seen through the top facet of the substrate, which is illuminated by a plane monochromatic wavefront at 632.8 nm wavelength. Propagation goes from left to right. The substrate has two channel waveguides separated 100 μm. Each channel waveguide has the same refractive index profile as shown in Fig. 4 and dimensions as showed in experimental case (Fig. 6). At the beginning of the left side it is possible to appreciate the diffraction light effects of the light coupling into the channel waveguide. The light from diffracted waves induce interference effects with light that propagates straightforward along the substrate. In addition, the diffracted waves suffer multiple reflections on the waveguides flanks, also light waves reflected in waveguides suffer transmission of light through them and the light get out of the image by the flanks. One can remark that waveguides can be identified observing both horizontal thin straight lines, close around the waveguides there are dark zones. In Fig. 7 one can

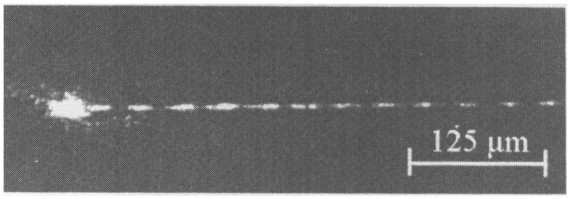

FIGURE 8. Photograph of the graded index channel waveguide. Ligth is launched through a single mode optical fiber, which is aligned for best coupling efficiency. Light propagates from right to left.

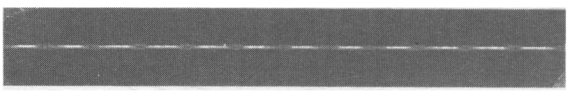

FIGURE 9. Result of the FFF-BMP simulation of light propagation with the same of figure conditions as in case showed in Fig. 8

see the complicated pattern of fringes because of the diffraction, multiple reflection and interference of light in the substrate. In accordance with the experimental image (Fig. 6), numerical simulation predicts the dark areas, which surround each waveguide, also at waveguides flanks predicts large stains of light.

Below we show the peculiarities of the light propagation in the channel waveguide associated with the coupling misalignment such as lateral offset and angular tilt between the waveguide and the coupled beam.

Figure 8 is a photograph of the top surface of the substrate with a straight graded index channel waveguide. Light from a He-Ne laser was launched into the channel waveguide with the aid of a single mode fiber, which is butted to the waveguide. Waveguide and optical fiber were aligned for the most efficient coupling for to have almost none lateral shifts and angular tilt.

Figure 9 shows the result of FFT-BPM simulation of the light propagation in a channel waveguide with the same refractive index profile as we had in our experimental samples. In the input plane of the waveguide, light had a Gaussian profile with a waist diameter of 8 μm, and neither lateral offset and angular tilt. Experimental and numerical simulation shown the periodical intensity variation along the waveguide that should be explained as a mode beating effect: the periodical variation in transverse intensity distribution caused by phase shift between the propagating modes. When two mode propagates in the waveguide, the spatial period of intensity variation, the mode beat length b, equals to the distance where these modes accumulate the 2π-phase shift, and $b = 2\pi/(k_1 - k_2)$, where k_1 and k_2 are the propagation constants. An unevenness or roughness in the waveguide can lead to optical losses due to scattering. In good quality optical material, such scattering centers are usually only found at the boundaries of the waveguide. At an uneven waveguide edge, the optical field will see irregular changes in refractive index and thus have a portion of the mode scattered out of the waveguide [33]. This allows to assume that the Fig. 8 shows the

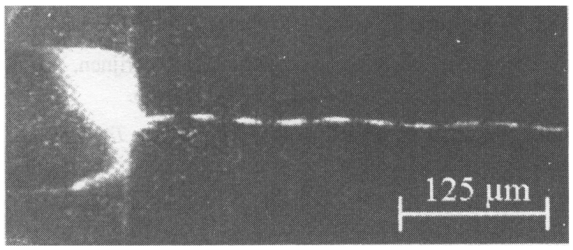

FIGURE 10. Photograph of the graded index channel waveguide propagating light at 632.8 nm. At left it is posible to see a optical fiber that has a lateral offset with respect to channel waveguide.

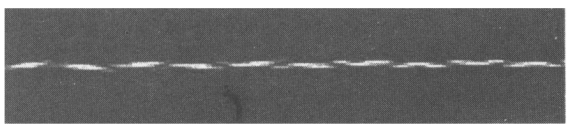

FIGURE 11. Results of the FFT-BMP simulation of light propagation with same figure conditions as in case showed in Fig. 11.

beating of the low-order modes HE_{00} and HE_{01}. Experiment shows that the beat length is $b = 36$ μm that gives $\Delta k = k_1 - k_2 = 174.5$ mm^{-1}. The data of Ref. 30 support our assumption that Fig. 8 shows the beating between the lowest index modes. In this work the propagation constants have been measured at same wavelength and for the channel waveguides fabricated with the same technique as we used for our experimental samples. According to this work the beat length for lowest modes is 27.5 μm, whereas the beat length is 13 μm for the beating of the HE_{00} and HE_{20} modes.

Figure 10 shows a photograph of the top surface propagation through a channel waveguide, it was taken when light was launched into waveguide with a lateral offset of $\sim$1–2 μm. On the left side of the photograph, it is possible to observe the substrate end surface and the output end of the optical fiber butted to the substrate.

Figure 11 presents the results of the FFT-BPM simulation similar to Fig. 9 but for 1 μm lateral offset and 1° angular tilt of the gaussian beam witch is coupled to the waveguide. The main difference between Figs. 10 and 11, and the previously discussed (Figs. 8 and 9), is a sinusoidal bending of the light trajectory in the waveguide. This effect should be attributed to the modal beating but in this case to the beating between EH_{00} and EH_{01} modes whereas the periodical variation of the intensity of scattered light has been attributed to the beating of EH_{00} and EH_{02} modes. The measurement of the bending period gives the beat length of approximately 120 μm, which corresponds to $\Delta k = 53$ mm^{-1}.

Our experiments show that our graded index waveguides support a multimode propagation at $\lambda = 632.8$ nm. The results of the numerical FFT-BPM simulation for longer wavelengths are shown in Fig. 12. One can see that the modal beat

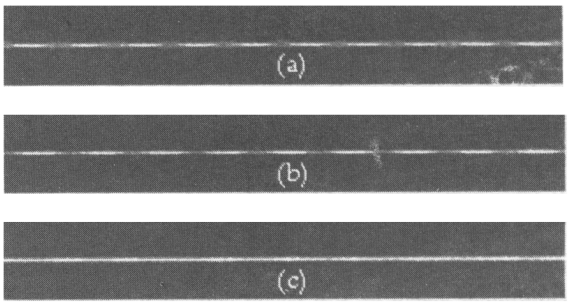

FIGURE 12. Results of the numerical simulation of the light propagation at the following wavelights: a) 850 nm, b) 1300 nm, and c) 1550 nm.

length increases with wavelength, thus Δk decreases as it is predicted by theory [34]. The mode beating is not observed at $\lambda = 1550$ nm. Therefore the waveguide supports the single mode propagation at that wavelength.

5. Conclusions

We have presented the results of the experimental and numerical investigation of the light propagation in the graded index channel waveguides. The samples for our experiments were fabricated by solid state diffusion of copper in glass substrates. The waveguides' index profile was calculated by solving numerically the equation for the ion exchange. These data have been used in numerical simulation of the light propagation by FFT-BPM. Our numerical results are in concordance with the experimental data and have allowed the analysis of the light propagation in the glass substrate with the waveguides as well as mode beating effects in the waveguides. We have observed experimentally the mode beating effects in the waveguides. We have observed experimentally the mode beating as periodical variation of the intensity scattered in the waveguide and as a spatial bending of the light trajectory. We used the numerical simulation to study the transition between the multimode and single mode operation of the waveguide with the wavelength increase. We have shown that waveguides are single mode at $\lambda = 1550$ nm.

Acknowledgments

The authors were supported by the CONACyT under project program 225080–5–28124A and CNRS-CONACyT cooperation program E.130.191. We are grateful to Ocean. Octavio Meillon-Menchaca for his photographic assessorship, to Mr. J. Dávalos for the assistance in the preparation of the samples and to Mr. Marco A. García Z. for his experimental assistance.

1. L.C. Barbosa, O.L. Aranha, and R. Srivastava, *Electron. Lett.* **32** (1996) 1919.
2. D. Cheng, J. Saarinen, H. Saarikoski, and A. Tervonen, *Optics Commun.* **137** (1997) 233.
3. R. Accornero *et al.*, *Electron. Lett.* **26** (1990) 1959.
4. Y. Chung, N. Dagli, and L. Thylen, *Electron. Lett.* **27** (1991) 2119.
5. A. Tervonen, *Integrated Optics Devices: Potential for Commercialization*, edited by S.I. Najafi and M.N. Ármenise, USA, (1997), SPIE, Vol. 2997, p. 202.
6. K.S. Chiang, *Optical and Quantum Electronics*, **26** (1994) s113.
7. M. Reinhard, *Integrated Optics: Design and Modeling*, (Artech House, USA, 1995).
8. A. Tervonen, *Glass Integrated Optics and Optical Fiber Devices*, edited by S.I. Najafi, San Diego, USA, (1994), Vol. CR53, p. 25.
9. W.C. Huang, C. Xu, C. Sai-Tak, and S.K. Chaudhuri, *J. Lightwave Tech.* **10** (1992) 295.
10. D. Yevick, *Optical and Quantum Electronics* **26** (1994) 185.
11. A.V. Komenko *et al.*, *Opt. Commun.* **150** (1998) 175.
12. C.A. Fuentes-Hernández and A.V. Khomenko, *Phys. Rev. Lett.* **83** (1999) 1143.
13. B. Hermansson, D. Yevick, W. Bardyszewski, and M. Glasner, *J. Lightwave Tech.* **8** (1990) 1866.
14. E. Montanari, S. Selleri, L. Vincetti, and M. Zoboli, *J. Lightwave Tech.* **16** (1998) 703.
15. Y. Arai, A. Maruta, and M. Matsuhara, *Opt. Lett.* **18** (1993) 765.
16. I.J. Craddock, C.J. Railton, and J.P. McGeehan, *IEEE Microwave and Guided Wave Lett.* **6** (1996) 40.
17. E.E. Kriezis and A.G. Papagiannakis, *J. Lightwave Tech.* **13** (1995) 692.
18. H.P. Nolting and R. März, *J. Lightwave Tech.* **13** (1995) 216.
19. F. Wijnands, H.J.W.M. Hoekstra, G.J.M. Krijnen, and R.M. de Ridder, *J. Lightwave Tech.* **12** (1994) 2066.
20. G.L. Yip and P.C. Noutsios, *IEEE Photonics Technology Lett.* **6** (1994) 543.
21. T. Rasmussen, J.H. Poulsen, and A. Bjarklev, *IEEE Photonics Technology Lett.* **5** (1993) 339.
22. P.C. Lee, D. Schultz, and E. Voges, *J. Lightwave Tech.* **10** (1992) 1832.
23. Y. Chung and N. Dagli, *IEEE J. Quantum Electron.* **27** (1991) 2296.
24. T.B. Koch, J.B. Davies, and D. Wickramasinghe, *Electron. Lett.* **25** (1989) 514.
25. D. Salazar *et al.*, *J. Modern Opt.* **46** (1999) 657.
26. J.A. Fleck Jr., J.R. Morris, and M.D. Feit, *Appl. Phys.* **10** (1976) 129.
27. M.A. Forastiere, G.C. Righini, G. Tartarini, and P. Bassi, *Linear and Nonlinear Integrated Optics*, edited by G.C. Righini and D.Yevick, Lindau, Fed. Rep. Germany, (1994), SPIE, Vol. 2212 p. 539.
28. J. Saijonmaa and D. Yevick, *J. Opt. Soc. Am.* **73** (1983) 1785.
29. H. Márquez *et al.*, *Appl. Opt.* **34** (1995) 5817.
30. D. Salazar, H. Porte, and H. Márquez, *Appl. Opt.* **36** (1997) 8987.
31. J. Van Roey, J. van der Donk, and P.E. Lagasse, *J. Opt. Soc. Am.* **71** (1981) 803.
32. A. Tervonen, S. Honkanen, and M. Leppinhalme, *J. Appl. Phys.* **62** (1987) 759.
33. H.P. Zappe, *Introduction to semiconductor integrated optics*, (Artech House, Boston, USA, 1995).
34. B.E.A. Saleh and M.C. Teich, *Fundamentals of Photonics*, (John Wiley & Sons, USA, 1991).